JOURNAL OF MATERIALS SCIENCE: MATERIALS IN MEDICINE **16** (2005) 679–685

Comparison of microstructural evolution in Ti-Mo-Zr-Fe and Ti-15Mo biocompatible alloys

S. NAG, R. BANERJEE, J. STECHSCHULTE*, H. L. FRASER
Center for the Accelerated Maturation of Materials, Department of Materials Science and Engineering, The Ohio State University, Columbus, Ohio, USA

The microstructural evolution and attendant strengthening mechanisms in two biocompatible alloy systems, the binary Ti-15Mo and the quaternary Ti-13Mo-7Zr-3Fe (TMZF), have been compared and contrasted in this paper. In the homogenized condition, while the Ti-15Mo alloy exhibited a single phase microstructure consisting of large β grains, the TMZF alloy exhibited a microstructure consisting primarily of a β matrix with grain boundary α precipitates and a low volume fraction of intra-granular α precipitates. On ageing the homogenized alloys at 600 °C for 4 h, both alloys exhibited the precipitation of refined scale secondary α precipitates homogeneously in the β matrix. However, while the hardness of the TMZF alloy marginally increased, that of the Ti-15Mo alloy decreased substantially as a result of the ageing treatment. In order to understand this difference in the mechanical properties after ageing, TEM studies have been carried out on both alloys in the homogenized and homogenized plus aged conditions. The results indicate that the ω precipitates dissolve on ageing in case of the Ti-15Mo alloy, consequently leading to a substantial decrease in the hardness. In contrast, the ω precipitates do not dissolve on ageing in the TMZF alloy and the precipitation of the fine scale secondary α leads to increased hardness.
© *2005 Springer Science + Business Media, Inc.*

1. Introduction

Human joints are prone to degenerative and inflammatory diseases that result in pain and stiffness of joints [1]. Approximately 90% of the population over the age of 40 suffers from some degree of degenerative joint disease [2]. When naturals joints cannot function optimally, they can be replaced by artificial biomaterials. The ideal recipe for a biomaterial to be used for implant application is excellent biocompatibility with no adverse tissue reactions, excellent corrosion resistance in the body fluid, high mechanical strength and fatigue resistance, low modulus, low density, and good wear resistance [1, 3].

In the early 1970's Titanium and its alloys started replacing stainless steel as an implant material. Though commercially pure (CP) Ti had corrosion resistance and tissue tolerance, it lacked load-bearing capabilities due to low strength. So CP Ti could not be used for load bearing applications such as total joint replacement. To improve upon this, Ti-6Al-4V ELI, adapted from the Ti-6Al-4V alloy which was developed for aerospace applications, was chosen. While the mechanical properties and corrosion resistance of this alloy are ideal for implant applications, studies have shown that both V and Al ions may cause long-term health problems. Moreover, the modulus of Ti-6Al-4V ∼110 GPa is substantially higher than that of bone (∼10–40 GPa) [1]. Finite-element simulations suggest that joint replacements may better simulate the femur in distributing stress if a lower modulus material is used [11, 12]. Large modulus mismatches cause insufficient loading of bone adjacent to the implant (*stress-shielding* phenomena) and eventual failure of the implant [13]. The high modulus of Ti-6Al-4V is attributable to the high volume fraction of the α phase in this alloy. Since the β phase in Ti alloys exhibits a significantly lower modulus than the α phase, there is a thrust towards the development lower modulus β-Ti alloys which retain a single β phase microstructure on rapidly cooling from high temperatures. Biocompatible β-Ti alloys include Ti-12Mo-6Zr-2Fe ('TMZF') [14], Ti-15Mo-5Zr-3Al [15], Ti-15Mo-3Nb-3O ('TIMETAL 21Srx') [16], Ti-14Nb-13Zr [17], Ti-35Nb-5Ta-7Zr ('TNZT') [18], and Ti-15Mo [19].

In this paper the microstructural development and attendant strengthening mechanisms in two of these β-Ti alloy systems, Ti-Mo-Zr-Fe, and binary Ti-15Mo will be investigated in detail.

2. Experimental procedure

The TMZF alloy was prepared by melting, 8 gm CP Ti, 1.2 gm Molybdenum (99.8% pure), 0.6 gm Zirconium

**Present address*: Department of Materials Science and Engineering, Cornell University, Ithaca, New York, USA.

(99.5% pure) and 0.2 gm Iron (99.97% pure). The Ti-15Mo alloy was prepared by melting appropriate amounts of Ti and Mo. The melting chamber was first evacuated and then back-filled with argon gas (pressure ∼13 inch Hg). Buttons, approximately 10 gms each, were melted in a copper hearth with a tungsten electrode. The buttons were re-melted 4 times in order to ensure chemical homogeneity. The arc-melted buttons were homogenized by heat-treating at 1100 °C for 7 days in a LINDBERG box furnace and then furnace cooled. Subsequently, the alloys were aged at 600 °C for 4 h and air-cooled. The homogenized and homogenized plus aged samples were mounted and mechanically polished using standard metallographic procedures.

Scanning Electron Microscopy (SEM) of these samples was performed using an FEI Sirion system equipped with a Field Emission Gun (FEG) emitter and an EDS detector. Transmission electron microscopy (TEM) was performed using a FEI/Philips CM200 TEM system operating at 200 KV accelerating voltage. Electron-transparent TEM specimens were prepared from site specific locations using the Focussed Ion Beam system (FEI Dual Beam 235 FIB). Microhardness tests were performed on these samples using a Vickers Micro Hardness Tester. The samples were tested using a load of 500 gf applied for 15 s. In addition to microhardness testing, in order to evaluate the modulus, these alloys were tested using nanoindentation in a Nanoindenter XP system from MTS Instruments. A Berkovich diamond indenter was used and measurements carried out for 2 μm deep indents. The modulus and hardness were evaluated from the unloading portion of the load-displacement data using standardized routines available in the MTS Testworks software.

3. Results and discussion

The average compositions of the TMZF alloy as measured using EDS in the SEM was Ti-13Mo-7Zr-3Fe while that of the binary alloy was Ti-15Mo. The overall microstructure of the Ti-15Mo alloy in the homogenized condition is shown in the SEM backscatter image inFig. 1(a). The microstructure primarily consists of relatively large grains of the β phase. Only a very small volume fraction of grain boundary α is present in this microstructure. A higher magnification image of grain boundary α precipitates at a triple junction of β grains is shown in Fig. 1(b). The average microhardness of the Ti-15Mo alloy in the homogenized condition is 379 VHN. The modulus as measured using nanoindentation was 112 GPa. The overall microstructure of the homogenized Ti-15Mo alloy after ageing at 600 °C for 4 h is shown inFig. 2(a). A fine scale secondary α precipitation occurs after the ageing treatment as shown in both Fig. 2(a) as well as the higher magnification image in Fig. 2(b). These finer scale α precipitates are homogeneously distributed throughout the β matrix. Fine scale α laths growing directly from the β grain boundary are clearly visible in Fig. 2(b). These and other microstructural observations suggest that the α laths formed after ageing, nucleated both at the grain boundaries as well as in the interior of the grains. In quite a few cases, clustering of morphologically similarly oriented laths was visible in the microstructure, an example of which is shown in Fig. 2(c). These laths are likely to exhibit similar crystallographic orientation too, making these clusters equivalent to colonies in $\alpha + \beta$ Ti alloys. The average microhardness of the homogenized Ti-15Mo alloy after ageing is 279 VHN while the modulus measured using nanoindentation is 124 GPa. The reduction in the microhardness and consequently the strength of the Ti-15Mo alloy after ageing is rather surprising since the homogeneous precipitation of the fine scale α after ageing is usually expected to increase the strength of the alloy. Therefore, further detailed investigations of the microstructural evolution in this alloy were carried out using transmission electron microscopy.

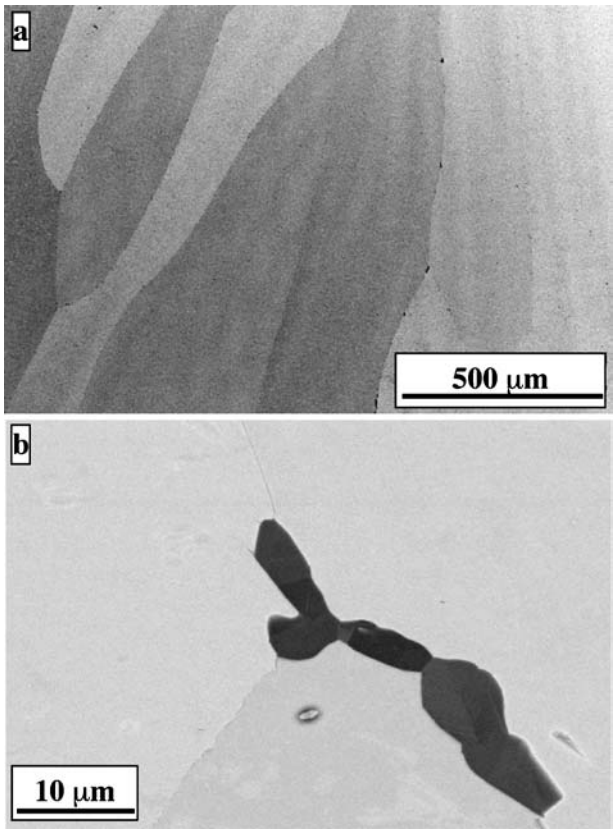

Figure 1 SEM backscatter images of the homogenized Ti-15Mo sample. (a) Overall microstructure showing large grains of β-Ti. (b) Higher magnification image showing the grain boundary α precipitates at a triple junction of β grains.

A bright-field TEM micrograph of the Ti-15Mo alloy in the homogenized condition, exhibiting the β matrix with a few small α precipitates, is shown inFig. 3(a). This TEM sample was prepared from a region within a β grain. A selected area diffraction (SAD) pattern from the β matrix is shown in Fig. 3(b). This SAD pattern can be consistently indexed as the [011] zone axis of the β phase. In addition to the primary β reflections in this diffraction pattern, additional sharp spots are visible at the 1/3{112} and 2/3{112} positions. These additional reflections arise from the precipitation of ω in the β matrix which are also clearly visible in the intensity line profile along the $g = \{21\text{-}1\}$ vector shown below Fig. 3(b).

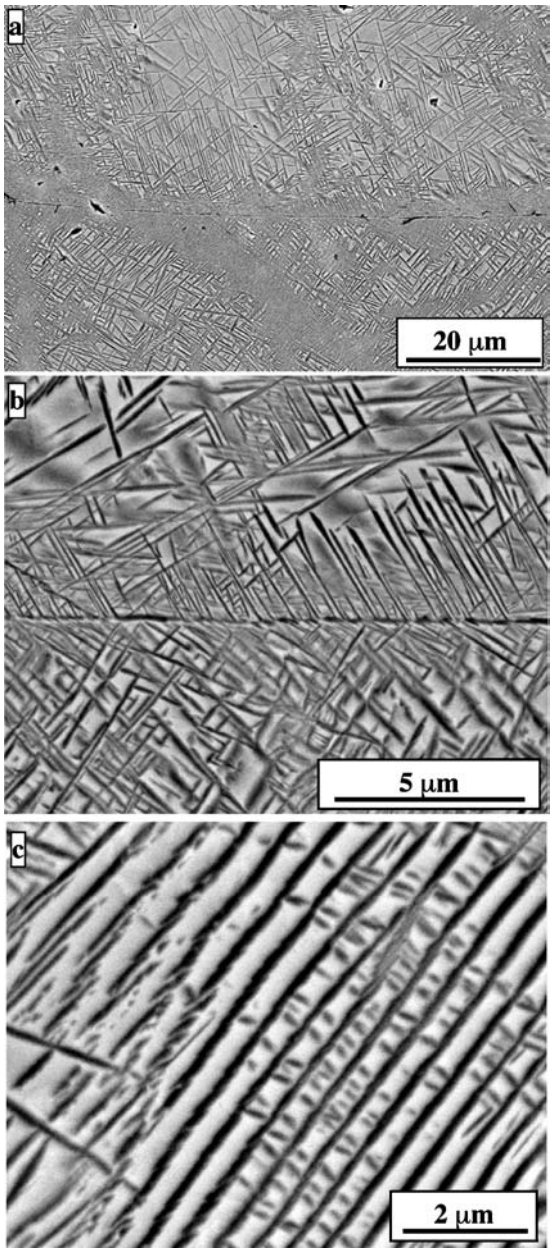

Figure 2 SEM backscatter images of the homogenized and aged Ti-15Mo sample. (a) Overall microstructure showing fine scale secondary α precipitation in the β matrix. (b) Higher magnification image showing the fine scale secondary α forming as a result of the ageing treatment. Note that there are α laths grow directly from the β grain boundary. (c) Higher magnification picture showing a cluster of α laths exhibiting the same orientation.

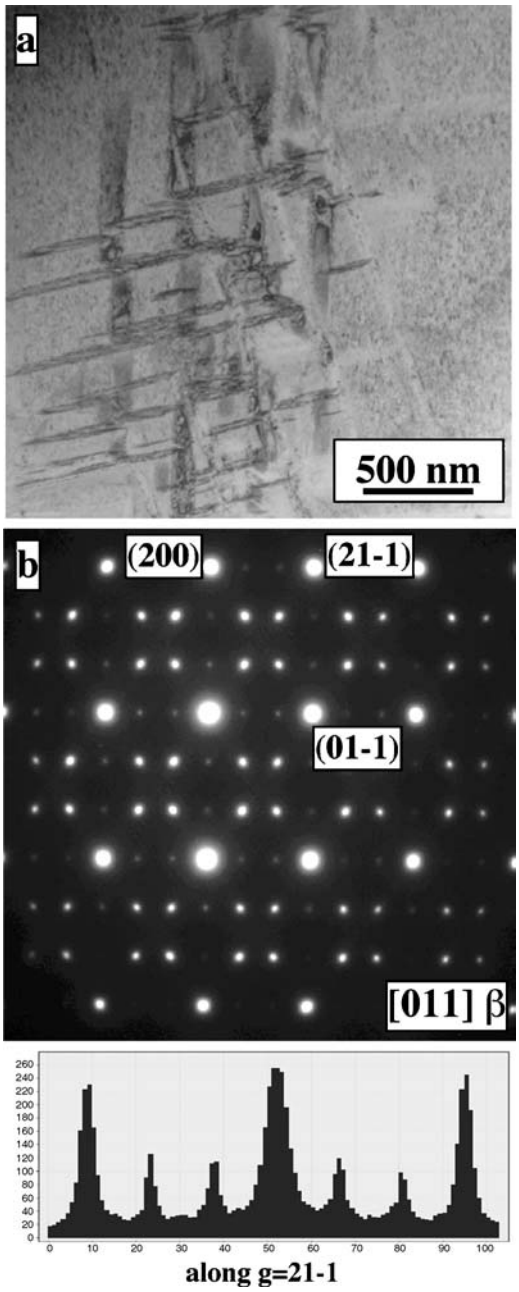

Figure 3 (a) Bright-field TEM image showing the β-matrix in the homogenized Ti-15Mo alloy. (b) [011] β SAD pattern and intensity profile along $g = 21\text{-}1$ reciprocal lattice vector.

After ageing at 600 °C for 4 h, the microstructure within the β matrix is shown in the bright-field micrographs, Figs. 4(a)–(c). Fine scale secondary α precipitates which formed as a result of the ageing treatment, are visible in these micrographs. These precipitates are of the same type as observed earlier in the SEM studies on the aged Ti-15Mo alloy (refer Figs. 2(b) and (c)).Fig. 4(a) is a low magnification bright-field image of laths of different crystallographic orientations exhibiting different diffraction contrasts in the same β grain. The higher magnification bright-field image, Fig. 4(b), shows a similar difference in the diffraction contrast of laths exhibiting different crystallographic orientations. In addition, there is clustering of laths of similar orientation, as encountered earlier in the SEM image shown in Fig. 2(c). In certain cases, the viewing direction was normal to a broad face of the α lath, an example of which is shown in Fig. 4(c). An SAD pattern of the [011] β zone axis in the homogenized plus aged Ti-15Mo alloy is shown in Fig. 4(d). This diffraction pattern has been recorded from a region of the matrix which did not include any fine scale secondary α precipitates. The additional reflections in this SAD pattern at the 1/3{112} and 2/3{112} positions, arising from ω precipitation, are substantially lower in intensity as compared with those in the homogenized alloy (Fig. 3(b)). The intensity line profile along $g = \{21\text{-}1\}$ vector, also shown in Fig. 4(d), confirms the same.

In case of the TMZF alloy, the overall microstructure of the alloy in the homogenized condition is shown in the SEM backscatter image,Fig. 5(a). The

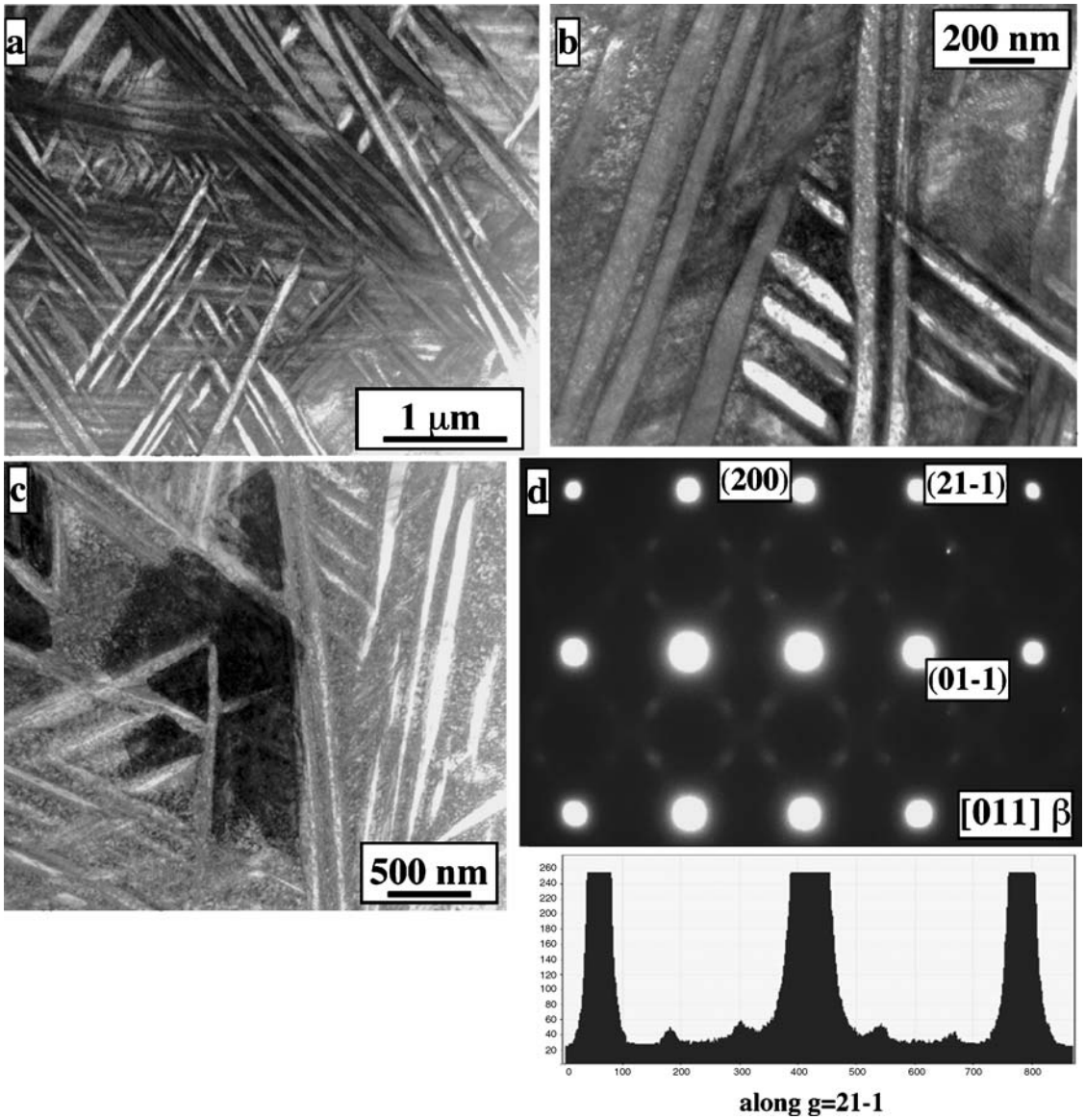

Figure 4 (a), (b) and (c) Bright-field TEM images showing the fine-scale secondary α within the β-matrix in the homogenized and aged Ti-15Mo alloy. (d) [011] β SAD pattern and intensity profile along $g = 21\text{-}1$ reciprocal lattice vector.

microstructure consists primarily of large β grains with grain boundary α precipitates and some intra-granular α precipitation at a relatively coarser scale. The grain boundary α precipitates and the intra-granular α are visible in the higher magnification SEM image shown in Fig. 5(b). The average microhardness of the homogenized TMZF alloy is 345 VHN and the modulus measured by nanoindentation is 89 GPa. Similar to the case of the Ti-15Mo alloy, the microstructure of the TMZF alloy after ageing at 600 °C for 4 h exhibited the homogeneous precipitation of a fine scale secondary α. The overall homogenized plus aged microstructure of TMZF is shown inFig. 6(a). Grain boundary α precipitates, intragranular primary α precipitates, and fine scale secondary α precipitates are shown in Fig. 6(b). It should be noted that precipitate-free zones are present on either side of the grain boundary for both the intragranular primary α as well as the fine scale secondary α. The extent of the precipitate-free zone is greater for the relatively coarser intra-granular α as compared with that for the fine scale secondary α, as seen in Fig. 6(b). Additionally, the intra-granular α precipitates also exhibit precipitate-free zones which are devoid of any fine scale secondary α precipitation, as shown in Figs. 6(b) and (c). Microhardness of the homogenized plus aged TMZF is 366 VHN while the modulus measured using nanoindentation is 118 GPa.

Details of the microstructural evolution in the TMZF alloy, in both homogenized as well as aged conditions, have been studied using TEM. Thus, a SAD pattern from the β matrix (not including any intra-granular α) of the homogenized TMZF alloy, which can be consistently indexed as the [011] β zone axis, is shown inFig. 7(a). In addition to the primary reflections arising from the β matrix, spots at 1/3 {112} locations are visible which indicate the presence of ω precipitates in this alloy. It should be noted that the additional rings in this diffraction pattern arise from the carbon film supporting the TEM specimen. A [011] β SAD pattern from the same alloy after ageing is shown in Fig. 7(b). In this case too additional reflections at the 1/3 {112} positions indicates the presence of ω precipitates. Intensity profiles along the $g = \{21 - 1\}$ vector on each of these diffraction patterns are shown below the respective

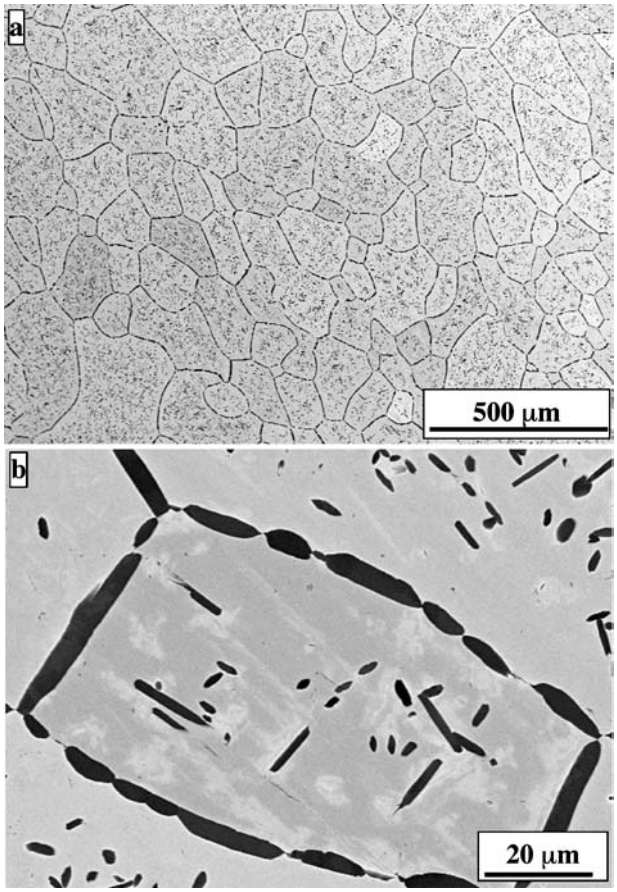

Figure 5 SEM backscatter images of the homogenized TMZF sample. (a) Overall microstructure showing grains of β-Ti. (b) Higher magnification image showing the grain boundary α precipitates and intragranular primary α precipitates.

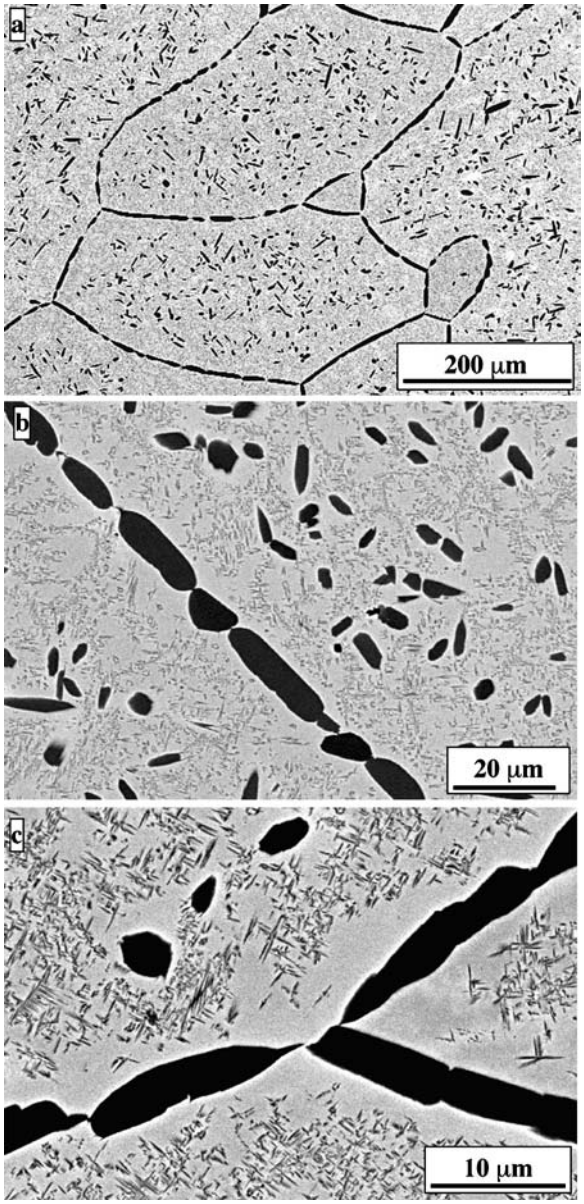

Figure 6 SEM backscatter images of the homogenized and aged TMZF sample. (a) Overall microstructure showing grains of β-Ti. (b) Higher magnification image showing the grain boundary α precipitates. (c) Higher magnification image showing the intragranular primary α precipitates and fine scale secondary α forming as a result of the ageing treatment. Note the precipitate-free zone next to the grain boundary α and the intragranular primary α precipitates.

patterns which substantiate the presence of the ω phase. The precipitation of the fine scale secondary α in the β matrix as a result of the ageing heat treatment is shown in the bright field TEM micrograph, Fig. 7(c).

Comparison of the microstructural evolution in the Ti-15Mo and TMZF alloys is directly indicative of the reasons behind the differences in the hardness and modulus of these alloys prior to and post the ageing heat treatment. Thus, in case of the Ti-15Mo alloy the homogenized condition consists of a large volume fraction of well-formed coarse ω precipitates, as evidenced from the distinct and intense reflections at the 1/3 and 2/3 {112} positions in the [011] β SAD pattern (Fig. 3(b)). After ageing at 600 °C for 4 h, the intensity of the ω reflections reduced substantially (Fig. 4(d)) indicating that the ω precipitates have undergone substantial dissolution and have been replaced by the fine-scale α precipitates. The substantial reduction in hardness accompanying this microstructural change clearly indicates that a more dominant role is played by the ω precipitates in strengthening the alloy as compared to the fine-scale secondary α formed after ageing. The role of ω precipitates in increasing the strength and hardness of Ti-15Mo to a greater degree as compared to α precipitates has been discussed previously by Bowen [20, 21]. The same microstructural change resulted in an increase in the modulus of the Ti-15Mo alloy from 112 GPa in the homogenized condition to 124 GPa after ageing, based on the results of nanoindentation measurements. The moduli of the β, α, and ω phases in Ti-15Mo have been reported to be 82, 124, and 165 GPa, respectively [21]. Using a simple rule of mixtures it can be estimated that the volume fraction of ω in the homogenized Ti-15Mo alloy is $\sim$0.5, assuming that there is negligible α in this condition. After ageing, the measured modulus is 124 GPa which is the same as that reported for the α phase in the literature [21]. The microstructural observations indicate the presence of a large volume fraction of fine scale secondary α precipitates in aged Ti-15Mo. Therefore, the increase in modulus after ageing can be attributed to the precipitation of a large volume fraction of secondary α in this alloy after ageing.

On the contrary, the TMZF alloy does not weaken on ageing but rather there is a marginal increase in the hardness of this alloy. In this case, the homogenized

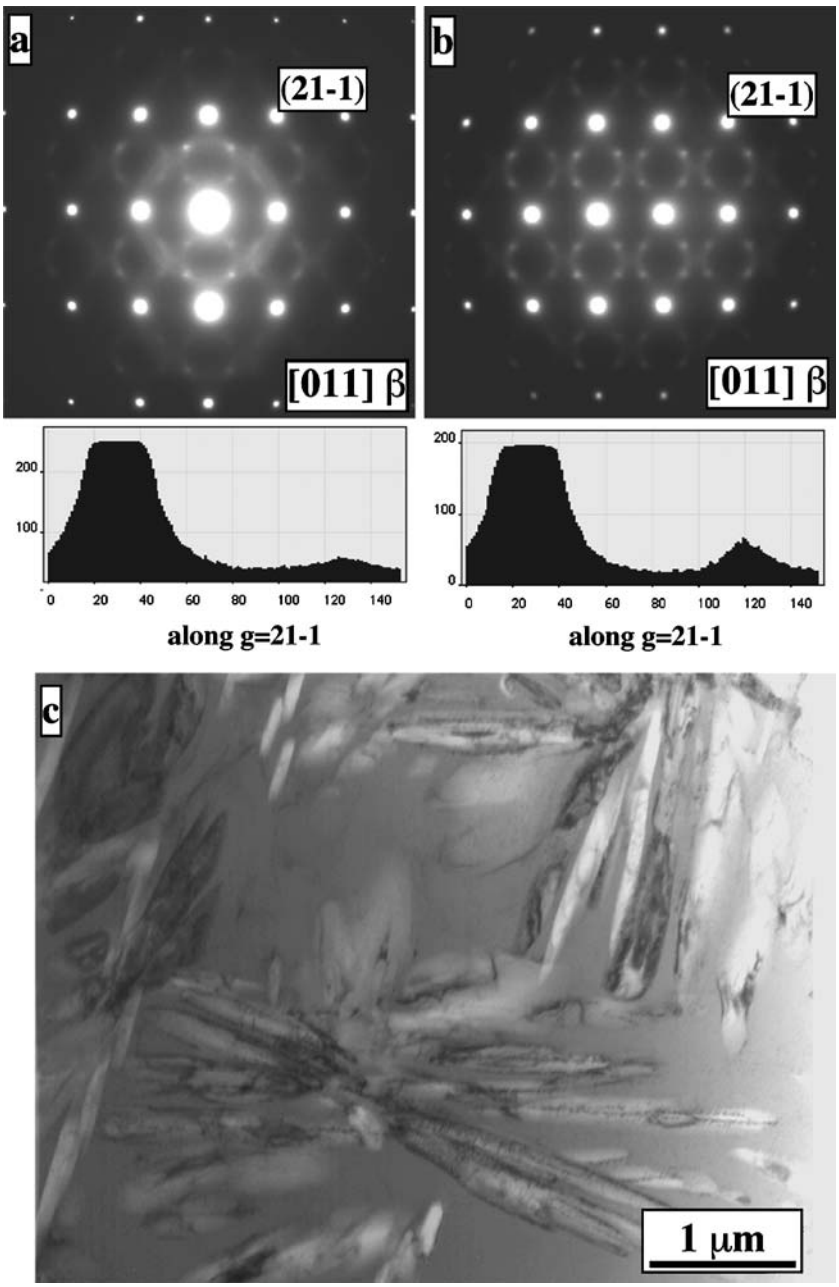

Figure 7 (a) [011] β SAD pattern and intensity profile along g = 21-1 reciprocal lattice vector in the homogenized TMZF alloy. Note that the intensity profile shows only one of the ω reflections. (b) [011] β SAD pattern and intensity profile along g = 21-1 reciprocal lattice vector in the homogenized and aged TMZF alloy. (c) Bright-field TEM image showing the fine-scale secondary α within the β-matrix in the homogenized and aged TMZF alloy.

condition consists of ω precipitates within the β matrix as well as some grain boundary and intra-granular α precipitates. After ageing at 600 °C for 4 h, the intensity of ω reflections does not reduce in the [011] β zone axis SAD pattern (compare Figs. 7(a) and (b)), but rather there appears to be a marginal increase in the intensity of ω reflections, as evident by comparing the intensity line profiles shown below the two figures. Therefore, the volume fraction of the ω phase does not seem to have depleted on ageing in case of the TMZF alloy. This is rather interesting since the TMZF alloy has 7 wt% Zr and the addition of Zr to binary Ti-V and Ti-Mo alloys has been reported to de-stabilize the ω phase [22]. While the role of the quaternary addition of 3 wt% Fe on the phase stability is not understood, the experimental evidence presented in this paper indicates that the ω phase does not dissolve after ageing at 600 °C for 4 h and consequently is not de-stabilized. A more detailed understanding of the phase stability in the TMZF alloy is the subject of future study. As far as hardness is concerned, no decrease in the strengthening arising from ω precipitates is expected in the aged condition as compared with the homogenized condition. However, the precipitation of the fine-scale secondary α as a result of ageing is likely to aid in the strengthening of the alloy and therefore, the higher hardness of the TMZF alloy after ageing can be rationalized. Similarly, the increase in modulus in this alloy after ageing can also be attributed to the precipitation of the α phase that exhibits a higher modulus as compared to the β phase [21].

4. Summary and conclusions

The microstructural evolution and attendant strengthening mechanisms in two biocompatible alloys based on β-Ti, Ti-15Mo and Ti-13Mo-7Zr-3Fe (TMZF), have been compared in this paper. In case of Ti-15Mo the dissolution of the ω precipitates negates the strengthening affected by the precipitation of the fine scale secondary α on ageing consequently leading to a reduction in the hardness of the alloy. The modulus, however, increases on ageing in the Ti-15Mo alloy primarily due to the precipitation of the high modulus secondary α phase. In contrast, in case of the TMZF alloy, the intensity associated with ω precipitation in the diffraction patterns is retained after ageing suggesting no decrease in the strengthening effect due to the ω phase. However, the precipitation of the fine scale secondary α on ageing does lead to a marginal increase in the strength of the alloy. The identification of the relative influences of different phases and microstructural features on the strength and modulus of these biocompatible alloys is expected to aid in the design of appropriate thermomechanical treatments for various applications.

References

1. M. J. LONG and H. J. RACK, *Biomater.* **19** (1998) 1621.
2. E. W. LOWMAN, *J. Amer. Med. Acad.* **157** (1955) 487.
3. K. WANG, *Mater. Sci. and Eng.* **A213** (1996) 134.
4. C. M. LEE, W. F. HO, C. P. JU and J. H. CHERN LIN, *J. Mater. Sci. Mater. Med.* **13** (2002) 695.
5. M. F. SEMLITSCH, H. WEBER, R. M. STREICHER and R. SCHÖN, *Biomater.* **13**(11) (1992) 781.
6. K.-H. BOROWY and K.-H. KRAMMER, "On the Properties of a New Titanium Alloy (Ti-5Al-2.5Fe) as Implant Material," Titanium 84': Science and Technology, Vol. 2 Munich, Deutsche Gesellschaft Für Metallkunde EV (1985) p. 1381.
7. S. G. STEINEMANN, "Corrosion of Surgical Implants—*in vivo* and *in vitro* Tests," Evaluation of Biomaterials, edited by G. D. Winter, J. L. Leray and K. de Groot (Wiley, New York, 1980).
8. S. G. STEINEMANN, "Corrosion of Titanium and Titanium Alloys for Surgical Implants," Titanium 84': Science and Technology, Vol. 2 Munich, Deutsche Gesellschaft Für Metallkunde EV, (1985) p. 1373.
9. S. RAO, T. USHIDA, T. TATEISHI, Y. OKAZAKI and S. ASAO, *Bio-med. Mater. Eng.* **6** (1996) 79.
10. P. R. WALKER, J. LEBLANC and M. SIKORSKA, *Biochemistry* **28** (1990) 3911.
11. E. CHEAL, M. SPECTOR and W. HAYES, *J. Orthop. Res.* **10** (1992) 405.
12. P. PRENDERGAST and D. TAYLOR, *J. Biomed. Eng.* **12**(5) (1990) 379.
13. W. F. HO, C. P. JU and J. H. CHERN LIN, *Biomater.* **20** (1999) 2115.
14. K. WANG, L. GUSTAVSON and J. DUMBLETON, "The Characterization of *Ti-12Mo-6Zr-2Fe*. A New Biocompatible Titanium Alloy Developed for Surgical Implants," Beta Titanium in the 1990's (The Mineral, Metals and Materials Society, Warrendale, Pennsylvania, 1993) p. 2697.
15. S. G. STEINEMANN, P.-A. MÄUSLI, S. SZMUKLER-MONCLER, M. SEMLITSCH, O. POHLER, H. -E HINTERMANN and S.-M. PERREN, "Beta-Titanium Alloy for Surgical Implants," Beta Titanium in the 1990's (The Mineral, Metals and Materials Society, Warrendale, Pennsylvania, 1993) p. 2689.
16. J. C. FANNING, "Properties and Processing of a New Metastable Beta Titanium Alloy for Surgical Implant Applications: TIMETAL^{TM} 21SRx," Titanium 95': Science and Technology (1996) p. 1800.
17. A. K. MISHRA, J. A. DAVIDSON, P. KOVACS and R. A. POGGIE, "Ti-13Nb-13Zr: A New Low Modulus, High Strength, Corrosion Resistant Near-Beta Alloy for Orthopaedic Implants," Beta Titanium in the 1990's (The Mineral, Metals and Materials Society, Warrendale, Pennsylvania, 1993) p. 61.
18. T. A. AHMED, M. LONG, J. SILVERSTRI, C. RUIZ and H. J. RACK, "A New Low Modulus Biocompatible Titanium Alloy," Titanium 95': Science and Technology, 1996) p. 1760.
19. K. WANG, *Mater. Sci. Eng. A* **213** (1996) 134.
20. A. K. BOWEN, *Scripta Metall.* **5** (1971) 709.
21. A. K. BOWEN, "On the Strengthening of Metastable β-Titanium Alloy by ω- an α-Precipitation," Titanium'80 Science and Technology, in Proceedings of the Fourth International Conference on Titanium, Kyoto, Japan, 1980) p. 1317.
22. J. C. WILLIAMS, B. S. HICKMAN and D. H. LESLIE, *Metall. Trans.* **2** (1971) 477.

Received 25 September 2003
and accepted 13 August 2004